

Stroboscopic detection of itinerant microwave photons

Hanna Zeller ^{1,*}, Lukas Danner,^{2,1} Max Hofheinz,³ Ciprian Padurariu,¹ Joachim Ankerhold,¹ and Björn Kubala^{2,1}

¹*Institute for Complex Quantum Systems and IQST, University of Ulm, 89069 Ulm, Germany*

²*German Aerospace Center (DLR), Institute of Quantum Technologies, 89081 Ulm, Germany*

³*Institut Quantique, Université de Sherbrooke, Sherbrooke, Québec J1K 2R1, Canada*

(Dated: March 18, 2026)

We present a novel scheme to detect itinerant microwave radiation at the single photon level. Using existing Josephson-photonics devices, where two microwave cavities are coupled by a dc-voltage biased superconducting junction, we theoretically show how to implement a stroboscopically repeated, near-projective measurement of a photon impinging on one of the cavities. Optimizing rate, duration, and strength of the measurement by flux control of the junction and developing a threshold protocol to detect the photon from a homodyne measurement of the radiation output of the other cavity, we achieve highly efficient detection with low dark counts. By cascading the detector with a preamplifier, where a similar two-cavity Josephson-photonics device acts as a photon multiplier, we can further improve the device to reach a detection efficiency of 88.5% with a dark count rate of $\sim 10^{-4}\gamma_a$, set by the resonance width γ_a of the absorbing cavity. These results for a multiplication factor of two suggest that near-unity efficiencies may be reached for higher multiplication factors.

I. INTRODUCTION

The efficient detection of single itinerant microwave photons remains a highly challenging task. This functionality is a key ingredient for many protocols and technologies in quantum information processing, quantum sensing, and quantum communication that rely on the quantum dynamics of superconducting electronic devices [1, 2]. More recently, they have also been used in magnetic resonance spectroscopy on single spins [3–5] or spin ensembles [6, 7] and in dark matter search experiments [8–10]. The requirements for different applications are as varied as the schemes of proposed and realized single-photon microwave detectors (see recent reviews [1, 2, 11] and references within). Schemes include bolometric detectors [12–16], which have not yet reached single-photon sensitivity, threshold detectors [10, 17–22], efforts to improve efficiency by arrays or cascades of detectors [23–26], various platforms incorporating qubits driven by complex pulse sequences [27–29], or devices specifically designed for resolving the photon-number distribution of a pulse with known arrival time [30].

Many proposals incorporate as the first step in the detection chain a cavity, on which the itinerant photon impinges. The state of the cavity is measured to detect if a photon has been absorbed, thus rendering the task of detecting an itinerant photon into the read-out of a quantum state. It has long been recognized [25, 31] that in any such proposal the measurement of the cavity’s state induces a Zeno-type backaction, which adversely affects the absorption of the incoming photon by the cavity, limiting the detection efficiency.

Here, we revisit this basic idea, but introduce three novel ingredients to such a scheme: Firstly, we show

within a toy-model, that stroboscopically repeated, instantaneous projective measurements of the cavity, which leave the cavity free to absorb the photon undisturbed in between the measurement instances, can achieve efficient detection. Secondly, we show that such a scheme can be realized utilizing existing *Josephson-photonics devices*, where two microwave resonators are coupled by a dc-voltage biased Josephson junction. These versatile devices can implement a variety of unconventional nonlinear single- or multi-photon drives [32–38] to create microwave radiation with interesting (quantum) properties [39–46], and have also been proposed [47, 48] and tested [49–51] for amplification and detection tasks. Here, they are used to implement a drive of the second cavity which (i) depends on the state of the first one and (ii) can be switched on and off via the flux bias of a superconducting quantum interference (SQUID) Josephson junction. Sending the itinerant photon on the first and monitoring the output of the second cavity by homodyne detection then mimics the aforementioned toy-model. Investigating the full simulation of the device’s quantum dynamics under a detailed measurement protocol, we find promising results with detection efficiency reaching 69.8% for realistic system parameters. Thirdly and finally, we will describe how our scheme can be improved by preamplifying the photon with the same type of Josephson-device, acting as a photomultiplier as described in [47, 48, 50]. Simulating a cascaded chain of a two-fold multiplier and a detector, we will show a detection efficiency which closely approaches simple estimates based on the toy-model, promising further improvements for higher multiplication factors.

* Contact author: hanna.zeller@uni-ulm.de

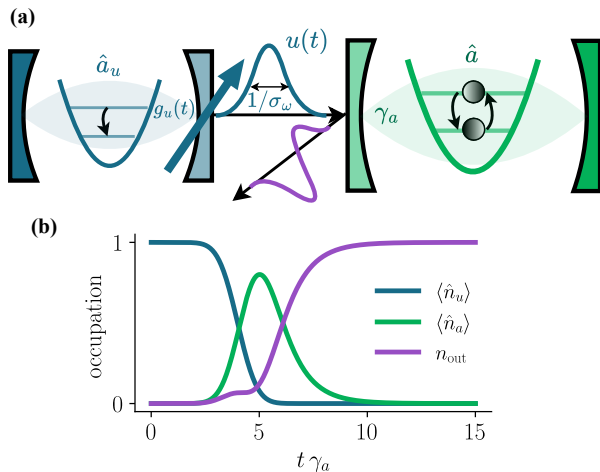


FIG. 1. (a) Effective description of a microwave cavity driven by an input field. The scenario is theoretically modeled by a cascaded Master equation involving an auxiliary cavity a_u that emits the quantum pulse $u(t)$ via a tunable decay coupling $g_u(t)$ (blue arrow). We assume a Gaussian mode $u(t) \sim e^{-(\sigma_\omega t)^2/2}$ with spectral width $\sigma_\omega = \gamma_a$ in a single-photon Fock state $|\psi\rangle_u = |1\rangle_u$. The input field is partly reflected and partly absorbed and re-emitted by the microwave cavity. (b) Occupations of auxiliary cavity a_u emitting the photon, cavity a which absorbs and subsequently emits the photon, and the integrated output $n_{out} = \int_0^t \langle \hat{L}_a^\dagger \hat{L}_a \rangle(t') dt'$. The plateau in n_{out} at $t\gamma_a \approx 4$ indicates destructive interference of contributions from direct reflection and from photon absorption and re-emission.

II. STROBOSCOPIC PROJECTIVE DETECTION OF AN ITINERANT PHOTON

As explained in the Introduction this paper will present a novel device enabling the detection of a single itinerant microwave photon by implementing a stroboscopically repeated, near-projective measurement of the occupation of a cavity, on which the itinerant photon impinges. If the photon is absorbed (as opposed to reflected) by the cavity, the projective measurement gathers information on the photon's existence. The described measurement process is non-destructive in the sense that subsequent to the measurement the photon decays from the cavity to its output transmission line and could, in principle, be subjected to further measurements [52]. Before presenting the experimental platform and the complete protocol in full, it is instructive to briefly investigate a simplified toy model that assumes a device-independent perfect projective measurement.

To start with, we need a full quantum description of the deterministic dissipative dynamics of a single photon impinging on a cavity and of the probabilistic quantum measurement process. The latter will then be replaced by the more complex description of the actual implementation of the measurement device in Secs. III and IV.

A single bosonic input field probing a quantum system is characterized by its carrier frequency ω_u , its incident time-dependent pulse shape $u(t)$, and by its quantum state (either a pure state $|\psi\rangle_u$ or a mixed state $\hat{\rho}_u$). We specifically consider the experimental scenario of a few-photon pulse impinging on a single microwave cavity with (rotating-frame) Hamiltonian $\hat{H}_0 = \hbar\Delta_a\hat{n}_a$ with loss rate γ_a , where $\Delta_a = \omega_a - \omega_u$ is the rotating-frame detuning. Theoretically, that situation is described following the framework presented by the Mølmer group [53, 54]. The approach relies on eliminating the explicit description of the propagating field by the introduction of an auxiliary cavity a_u with a time-dependent loss-rate $g_u(t)$, see Fig. 1(a), specifically constructed to emit the quantum pulse $u(t)$ [53, 54]. A cascaded Master equation with Hamiltonian $\hat{H} = \hat{H}_0 + (i\frac{\hbar}{2}g_u(t)\sqrt{\gamma_a}\hat{a}_u^\dagger\hat{a} + \text{h.c.})$ and single Lindblad operator $\hat{L}_a = g_u^*(t)\hat{a}_u + \sqrt{\gamma_a}\hat{a}$ ensures the uni-directional influence of the quantum pulse driving the cavity. To demonstrate this effective description, the occupations of a_u and a as well as the integrated output of the system, when a photon in a resonant Gaussian mode impinges on a are shown in Fig. 1(b). The photon is emitted from a_u (blue), impinges on cavity a where

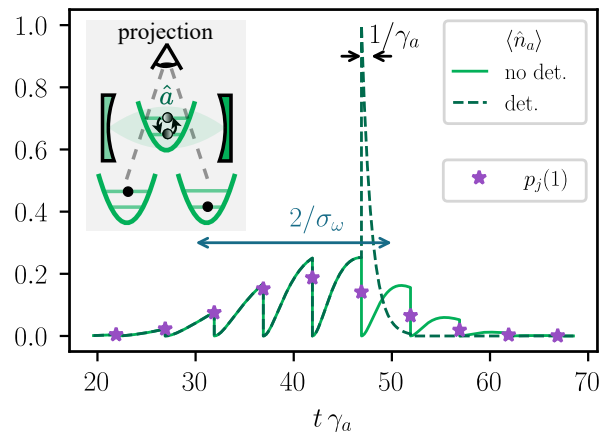


FIG. 2. Stroboscopic projective measurements (performed with frequency $\gamma_m = 0.2\gamma_a$) of a microwave cavity a that is subject to an impinging resonant Gaussian single-photon pulse ($\sigma_\omega/\gamma_a = 0.1$). Each measurement projects the cavity's state either to $|1\rangle_a$ (i.e. the photon is detected) or to $|0\rangle_a$, where the photon remains undetected (c.f. schematic setup in the inset). The solid line shows a trajectory where the photon was never detected, while the dashed trajectory detects the photon in the measurement at $t_{m,j} = 47/\gamma_a$, where the (total) state is projected to $|\psi\rangle = |01\rangle_{u,a}$. Because of the subsequent exponential decay, the cavity occupation will be (with very high probability) projected to vacuum in the following measurement. The probability to find the photon at measurement j , $p_j(1) = p_j(O_j = 1, O_k = 0 \forall k < j)$ is indicated by purple markers, while the total photon detection probability is $\eta = 67\%$. The y-axis shows both the occupation and the probability (same scale). [Parameters: $\gamma_m = 0.2\gamma_a$, $\sigma_\omega = 0.1\gamma_a$, $\Delta_a = 0$.]

it is partly reflected and partly absorbed and re-emitted (green) to the environment, where the integrated output finally reaches unity (violet).

Projective measurements performed on the cavity a are added by simulating the system up to the point of a projective measurement at $t_{m,j}$ with the same Lindblad master equation for a_u and a . Then, depending on the outcome $O_j \in \{0, 1\}$ of the measurement j , the new state $\hat{\rho}'$ of the system is given by

$$\hat{\rho}'(t_{m,j}|O_j) = \frac{\hat{P}_{O_j} \hat{\rho}(t_{m,j}) \hat{P}_{O_j}}{\text{tr} [\hat{P}_{O_j} \hat{\rho}(t_{m,j}) \hat{P}_{O_j}]} \quad (1)$$

with $\hat{P}_1 = \mathbf{1}_u \otimes |1\rangle\langle 1|_a$ when a photon is detected, and $\hat{P}_0 = \mathbf{1} - \hat{P}_1$ if not. Subsequently, the state $\hat{\rho}'$ is evolved with the Lindblad master equation up to the next measurement.

Fig. 2 shows two distinct trajectories with stroboscopically repeated projective measurements. When a mea-

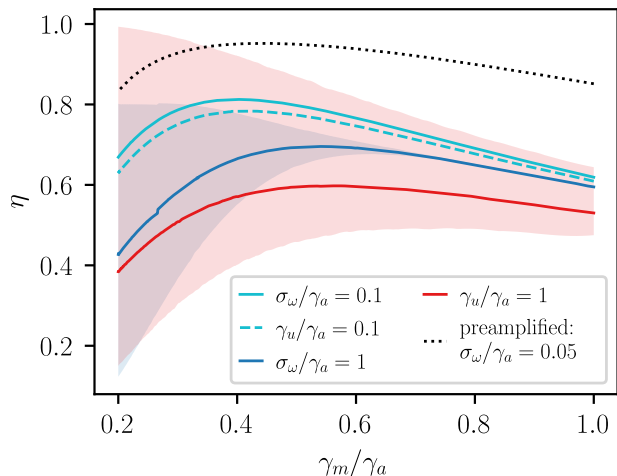


FIG. 3. Detection probability η depending on the measurement rate γ_m for different pulse shapes. The curves were averaged over several measurement positions relative to the pulse. Shaded regions indicate the range of detection probabilities depending on the relative measurement position.

A maximum detection probability of $\eta = 81\%$ can be achieved for a measurement rate $\gamma_m = 0.4\gamma_a$ for spectrally narrow and resonant Gaussian input pulses (solid light blue, $\sigma_\omega = \gamma_a/10$), while it peaks at $\eta = 78\%$ for resonant exponential input pulses, $u(t) = \sqrt{\gamma_u} \theta(t) e^{-\gamma_u t/2}$ (where $\gamma_u = \gamma_a/10$, dashed). For spectrally broader Gaussian input pulses ($\sigma_\omega = \gamma_a$, dark blue line and region), and for a time-reversed exponential pulse $u(t) = \sqrt{\gamma_u} \theta(-t) e^{\gamma_u t/2}$ ($\gamma_u = \gamma_a$, red line and region), the maximum detection probability is significantly smaller. Due to the stricter time confinement of those pulses, the position of the measurements relative to the pulses' arrival time strongly influences the total detection probability, especially for low measurement frequencies. A preamplification of a resonant single-photon Gaussian input pulse ($\sigma_\omega = \gamma_a/20$) with multiplication factor $n = 2$ (c.f. Sec. IV) enables near-deterministic detection, $\eta = 95\%$.

surement finds no photon as for all measurements of the first trajectory (solid line), the cavity occupation, \hat{n}_a , resets to 0 and has to be driven up by the incoming photon pulse again. When a photon is found as in the measurement at $t = 47/\gamma_a$ of the second trajectory (dashed line), the state of the system is projected to $|01\rangle_{u,a}$. Afterwards, the photon decays from the cavity a to the environment. As the quantum pulse does not contain any photons after the detection of the photon in a , the pulse does not drive cavity a thereafter.

The probability to miss the photon in measurement j , conditional on the previous measurement outcomes, is $p_j(O_j = 0|\{O_k\}, k < j) = \text{tr} [\hat{\rho}(t_{m,j}) \hat{P}_0]$. Thus, the photon detection probability η of finding the photon in any of the M measurements, is given by $\eta = 1 - \prod_{j=0}^M p_j(0|O_k = 0 \forall k < j)$. That overall detection probability η depends on the pulse shape $u(t)$, the measurement rate $\gamma_m = 1/t_{\text{dist}}$, where t_{dist} is the time between measurements, and the position of the measurements relative to the quantum pulse. The dependence of η on γ_m is depicted in Fig. 3 for several pulse shapes (Gaussian, rising/decaying exponential). To detect a photon with high probability, it has to be resonant in order to enter the cavity efficiently (cf. the solid curves in light/dark blue for Gaussian pulses with small/large frequency spread), and measurements should occur frequently enough, so that it is not missed. However, measuring too frequently freezes the cavity in the empty state by the quantum Zeno effect: the initially quadratic increase in occupation after an unsuccessful measurement leads to a very small probability for a measurement following shortly after. This decrease in probability cannot be compensated by the increased number of measurements. In accordance with these simple arguments, we find an optimum at a moderate detection frequency of $\gamma_m \approx 0.4\gamma_a$ (for resonant pulses).

Given resonant pulses, their exact pulse shape is less important, as exemplified by comparing the solid light blue to the dashed light blue line in Fig. 3; the latter stemming from the (natural) exponential decay of an input cavity with constant decay rate.

It is also instructive to consider a single-photon pulse shaped to the time-reversed version of the natural exponential decay, that has recently raised attention, as it can be perfectly absorbed [55]. A cavity with matching decay rate will reach unity occupation at the time the pulse stops, see App. A, before it eventually decays. Were a single measurement to occur at that time of unity occupation, it would result in deterministic detection (upper left corner of the red shaded region in Fig. 3). However, if the arrival time of the photon is unknown, the resulting detection probabilities have to be averaged over all possible positions of the stroboscopic measurements (shaded vertical range), and the resulting averaged probability (solid red line) is quite small for that pulse shape.

III. A JOSEPHSON-PHOTONICS DEVICE IMPLEMENTING PROJECTIVE DETECTION

Aiming to implement the projective measurement of the occupation of a cavity a , discussed in its idealized abstract version in the previous section, we use the two-cavity Josephson-photonics device (JPD) shown in Fig. 4. Two cavities are connected in series with a dc-voltage biased Josephson junction, such that the system can be described by the Hamiltonian [36]

$$\hat{H}_{\text{JPD}} = \hbar\omega_a \hat{a}^\dagger \hat{a} + \hbar\omega_b \hat{b}^\dagger \hat{b} - E_J \cos[\omega_{\text{dc}}t + \alpha_0(\hat{a}^\dagger + \hat{a}) + \beta_0(\hat{b}^\dagger + \hat{b})], \quad (2)$$

where the dc-voltage can be associated with a driving frequency $\omega_{\text{dc}} = 2eV_{\text{dc}}/\hbar$. In such a device, the tunneling of a Cooper pair across the junction (represented by the $e^{\pm i\omega_{\text{dc}}t}$ terms in the Hamiltonian) couples to processes containing any number of photon creation/destruction events in the two cavities, $[\alpha_0 \hat{a}^\dagger]^n [\alpha_0 \hat{a}]^m [\beta_0 \hat{b}^\dagger]^s [\beta_0 \hat{b}]^t$ ($m, n, s, t \in \mathbb{N}_0$), stemming from the expansion of the cos-term in Eq. (2), where α_0, β_0 are the zero-point fluctuations of the phase variables of cavities a, b [32, 33, 36]. Relevant are those terms, where the energy of the tunneling Cooper pair closely matches the energy of created and destroyed photons. For instance, a pair of entangled photons in cavity a and b may be created, if $\omega_{\text{dc,ent}} = \omega_a + \omega_b$ [40, 45, 56]. Here, we tune the dc-bias to $2eV_{\text{dc}} = \hbar\omega_{\text{dc}} \approx \hbar\omega_b$ such that there is a dominant low-order term, $\cos(\omega_{\text{dc}}t)\beta_0(\hat{b}^\dagger + \hat{b})$, driving cavity b linearly, while cavity a appears as a mere bystander to this process. However, from the argument above it is obvious that this simple process is modified by other resonant processes involving arbitrary

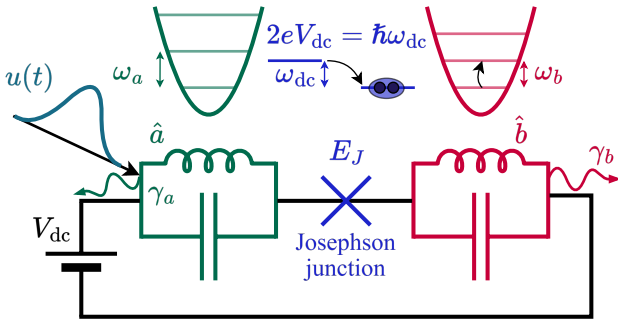


FIG. 4. Schematic electrical circuit of a Josephson-photonics device consisting of two microwave cavities connected in series with a dc-biased Josephson junction. By tuning the voltage to the single-photon resonance of cavity b , $\omega_{\text{dc}} = \omega_b$, each Cooper pair (CP) tunneling through the junction effectively creates one photon in b . The linear driving of cavity b is renormalized by virtual excitations [c.f. the Bessel functions in Eq. (3)], and thereby depends on the state of cavity a . An impinging quantum pulse modifies the state of cavity a , which effectively modulates the driving and thus the quantum state of cavity b .

powers of $\hat{n}_a = \hat{a}^\dagger \hat{a}$ and \hat{n}_b which (i) make the single-photon driving of b nonlinear, and, more importantly for this work, (ii) make the drive of cavity b depend on the occupation of cavity a .

To isolate the so-renormalized resonant process, we move to the rotating frame and apply a rotating-wave approximation (RWA) yielding

$$\begin{aligned} \hat{H}_{\text{RWA}} &= \hbar\Delta_a \hat{a}^\dagger \hat{a} + \hbar\Delta_b \hat{b}^\dagger \hat{b} \\ &- i \frac{E_J^* \beta_0}{2} : [\hat{b} - \hat{b}^\dagger] J_0(2\alpha_0 \sqrt{\hat{n}_a}) \frac{J_1(2\beta_0 \sqrt{\hat{n}_b})}{\beta_0 \sqrt{\hat{n}_b}} : \\ &\approx \hbar\Delta_a \hat{a}^\dagger \hat{a} + \hbar\Delta_b \hat{b}^\dagger \hat{b} - i \frac{E_J^* \beta_0}{2} [\hat{b} - \hat{b}^\dagger] (1 - \alpha_0^2 \hat{n}_a) \end{aligned} \quad (3)$$

with $\Delta_a = \omega_a - \omega_{a,\text{rot}}$ (usually set by the input pulse, i.e., $\omega_{a,\text{rot}} = \omega_a$), $\Delta_b = \omega_b - \omega_{\text{dc}}$ and $E_J^* = E_J e^{-(\alpha_0^2 + \beta_0^2)/2}$. The approximation leading to the last line assumes negligible nonlinearities in the driving of b (i.e. $\beta_0 \sqrt{\langle \hat{n}_b \rangle} \ll 1$) and a single photon in cavity a , for which case the Bessel function, $J_0(2\alpha_0 \sqrt{\hat{n}_a})$, can be projected to the $n_a = 0, 1$ subspace. The moment-occupation coupling $\hat{p}_b \hat{n}_a$ realizes a driving strength for cavity b which depends on the

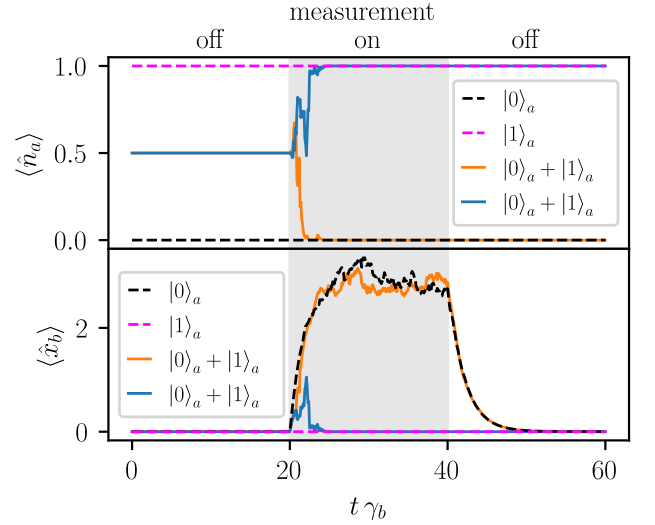


FIG. 5. Measuring a closed cavity a , $\gamma_a = 0$, in a Josephson-photonics setup. The coupling E_J is switched on between $t\gamma_b = 20$ and $t\gamma_b = 40$. The top panel shows the occupation of cavity a , while the bottom panel shows the quadrature $\langle \hat{x}_b \rangle$ of cavity b . If cavity a is empty, cavity b is driven to a (near-)coherent state $|\beta = 1.6\rangle$ and returns to vacuum when E_J is switched off (dashed black lines). For $\alpha_0 = 1$ and when $|\psi\rangle_{0,a} = |1\rangle$, the effective driving strength of b vanishes, such that b stays in vacuum irrespective of the coupling (dashed magenta lines). When cavity a starts in a coherent superposition $|\psi\rangle_{0,a} = (|0\rangle + |1\rangle)/\sqrt{2}$, the measurement projects its state to either $|0\rangle_a$ (solid orange lines) or $|1\rangle_a$ (solid blue lines) with a probability of 1/2 each.

[Parameters: $\gamma_b = 1$, $\beta_0 = 0.3$, $\Delta_a = \Delta_b = 0$, $E_J^* \beta_0 / (\hbar\gamma_b) = 1.6$.]

state of cavity a . As direct consequence, a photon detection scheme can be devised that monitors observables of b , such as homodyne or heterodyne quadrature measurements, and thereby acquires information on the occupation of a . In the following, we will lay out how this basic idea is extended to a full scheme of stroboscopic detection of itinerant photons. First, we will sketch how a single near-projective measurement of the state of a closed ($\gamma_a \equiv 0$) cavity a is realized, by switching on a strong Josephson coupling, E_J , and thus an \hat{n}_a -dependent driving of cavity b in the JPD setup of Fig. 4 [57]. To infer the information on \hat{n}_a , a convenient measurement observable has to be extracted from the monitored output of b . After characterizing a single measurement, we will turn in Sec. III B to stroboscopically-repeated fast measurements of an open cavity a , on which a single-photon

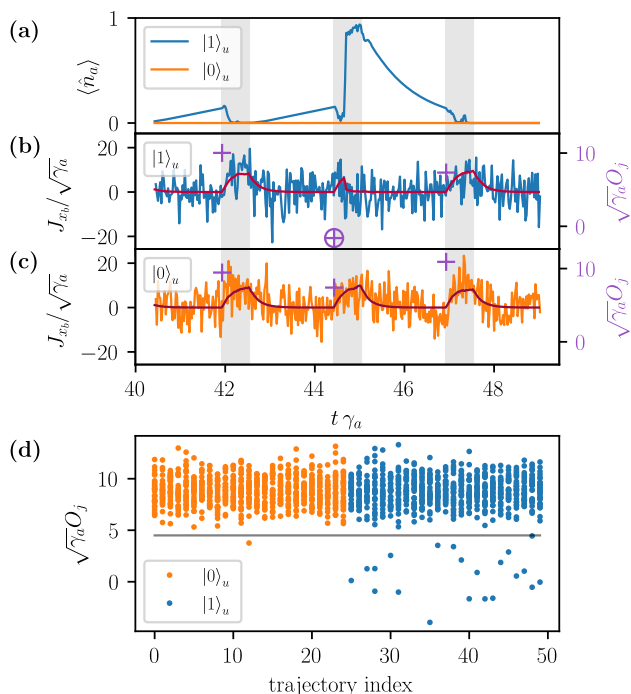


FIG. 6. (a) Occupation \hat{n}_a with (blue) and without (orange) resonant Gaussian photon input for three consecutive measurements (grey areas). Absorption of the photon happens in the second measurement shown, where a is projected to $|1\rangle$. (b)/(c) Measurement outcome J_{x_b} (blue/orange) and expectation value $\sqrt{\gamma_b}\langle\hat{x}_b\rangle$ without noise (red) corresponding to the two trajectories shown in (a). The outcomes O_j of the three measurements are plotted as purple crosses (scale on the right). The measurement where a photon is detected shows a significantly smaller outcome O_j (circled cross). (d) Measurement outcomes for several trajectories with/without (blue/orange) input photon, where each trajectory was measured 31 times (vertical stacks). Data points below a chosen threshold (gray line) are classified as detection events.

[Parameters: $\gamma_m/\gamma_a = 0.4$, $t_m\gamma_a = 0.6$, $\sigma_w/\gamma_a = 0.1$, $t_0\gamma_a = 40$, $\gamma_b/\gamma_a = 10$, $\alpha_0 = 1$, $\beta_0 = 0.3$, $\Delta_a = \Delta_b = 0$, $E_J^*\beta_0/(\hbar\gamma_b) = 1.6$.]

pulse impinges.

A. Homodyne detection

We want to implement a near-projective measurement of cavity a by monitoring the x -quadrature of the microwave-radiation output of cavity b . To describe such a homodyne measurement, we follow the standard quantum-optics approach [58] and employ the stochastic master equation,

$$d\hat{\rho}(t) = d_1\hat{\rho}dt + d_2\hat{\rho}dW, \quad (4)$$

with the Wiener increment

$$\langle dW \rangle = 0, \quad \langle dW^2 \rangle = dt. \quad (5)$$

The *deterministic* part of the master equation is given by

$$d_1\hat{\rho} = -i[\hat{H}, \hat{\rho}] + \mathcal{D}[\hat{C}]\hat{\rho} + \mathcal{D}[\hat{S}]\hat{\rho}, \quad (6)$$

with

$$\mathcal{D}[\hat{L}]\hat{\rho} = \frac{1}{2} [2\hat{L}\hat{\rho}\hat{L}^\dagger - \hat{\rho}\hat{L}^\dagger\hat{L} - \hat{L}^\dagger\hat{L}\hat{\rho}]. \quad (7)$$

For our set-up, the unmonitored operator is $\hat{C} \equiv \hat{L}_a = \sqrt{\gamma_a}\hat{a}$ ($+g_u^*(t)\hat{a}_u$), see above, as we do not observe cavity a directly, while the output of b is monitored, $\hat{S} \equiv \hat{L}_b = \sqrt{\gamma_b}\hat{b}$. The Hamiltonian \hat{H} is the full model Hamiltonian, potentially including the cascaded auxiliary cavity.

The *stochastic* part is calculated by

$$d_2\hat{\rho} = \hat{S}\hat{\rho} + \hat{\rho}\hat{S}^\dagger - \text{tr}[\hat{S}\hat{\rho} + \hat{\rho}\hat{S}^\dagger]\hat{\rho}. \quad (8)$$

The stochastic quantum master equation then yields individual trajectories for the quadrature measurement,

$$J_{x_b} = \langle \hat{L}_b + \hat{L}_b^\dagger \rangle + \frac{dW}{dt}, \quad (9)$$

where the derivative of the Wiener increment simulates vacuum noise associated with each measurement run. These trajectories have the same noise properties as an experiment, where the radiation leaking out of b is fed into a phase-sensitive quantum-limited amplifier, whose output is subsequently recorded and processed classically.

To implement a projective measurement of cavity a , the Josephson coupling E_J is switched on, so that cavity b is driven on its fundamental single-photon resonance, $\Delta_b = \omega_b - \omega_{dc} = 0$, assuming a perfectly stable dc-voltage for the purpose of this publication [59]. According to Eq. (3), if cavity a is in vacuum, cavity b is driven into the coherent state $|\beta\rangle$ with $\beta = E_J^*\beta_0/(\hbar\gamma_b)$. The effective driving of b is reduced when cavity a is occupied by a photon and, indeed, vanishes for $\alpha_0 = 1$. The results of such measurements on a closed (i.e. $\gamma_a = 0$) cavity a

prepared in different initial states are shown in Fig. 5. After E_J is switched on, the quadrature $\langle \hat{x}_b \rangle$ (shown in Fig. 5 for individual trajectories without the Wiener increment) quickly approaches a finite value or zero, while the state of the cavity is projected to the corresponding measurement-eigenstates $|0\rangle$ or $|1\rangle$, if the initial state is a superposition $|\psi\rangle_a = (|0\rangle + |1\rangle)/\sqrt{2}$.

B. Stroboscopically-repeated measurements

Keeping the Josephson coupling constantly on, $E_J \neq 0$, is not conducive to our ultimate goal of detecting itinerant single-photon pulses, as it will strongly reduce the probability that the incoming photon is absorbed by the cavity. This can be seen as being due to a strong dephasing noise acting on cavity a caused by the fluctuations of the state of cavity b [c.f. the $(\hat{b} - \hat{b}^\dagger) \hat{n}_a$ term in the Hamiltonian (3)] or as an effect analogous to the quantum-Zeno-like reduction of the detection probability for the regime of projective measurements with high rate in Fig. 3. In consequence, we turn to stroboscopically switching E_J on only for a short measurement interval, just long enough to determine the state in a , and repeat such near-projective measurements with a frequency similar to the optimal frequency for our toy-model's projective measurements in Fig. 3. This requires a separation of time scales, $\gamma_b \gg \gamma_a$, so that b adapts to the state in a very quickly and thus mimics the ideal instantaneous projective measurement.

Fig. 6(a-c) gives two example trajectories, one with and one without an incoming photon, where three consecutive measurements are performed in the manner just described. Shown are the occupation of cavity a [in Fig. 6(a)] and in (b-c) the measurement signal, the observed quadrature $\langle \hat{x}_b \rangle$ with the explicit noise term of Eq. (9) (blue and orange), and for comparison without that term (solid red lines).

Considering first the trajectory without photon input (dark green line in (a) and (c)), we see how cavity b is driven towards its finite-quadrature steady state during the measurement, while relaxing back to the ground state when E_J is off again. With a single-photon input, similar behavior of cavity b is observed for the first and third measurement shown, where the state in a is projected to $\approx |0\rangle$ as seen in (a). For the second measurement on the other hand, cavity a is projected to $\approx |1\rangle$ and the quadrature of $\langle \hat{x}_b \rangle$ remains closer to 0. However, the noise on the actual observed J_{x_b} , makes the distinction between measurement outcomes harder.

To distinguish the difference of the signals hidden in background noise, J_{x_b} is integrated

$$O_j = \int_{t_{j,\text{start}}}^{t_{j+1,\text{start}}} J_{x_b}(t)w(t)dt \quad (10)$$

with a weight function $w(t)$ to obtain a single real value O_j for each measurement [indicated by +-markers (b)

and (c) of Fig. 6]. Low values of O_j as in the second measurement of the middle panel indicate a successful photon detection. The *weight function* $w(t)$, shown and discussed in more detail in Appendix B, disregards values at the start and long after the measurement, where the expected observed quadrature of b does not depend on the state of a , while peaking where that dependence is maximal.

For the *classification of measurements* a threshold is defined, below which a photon detection event is declared. Measurement outcomes O_j for some trajectories without (orange points on the left) and with input (right) are shown in Fig. 6(b) with a threshold line set to classify as many measurements correctly as possible.

With the chosen circuit parameters, weight function, and threshold definition we obtain a detection efficiency of $\eta = 69.8\%$ coming quite close to detection probability of the idealized projective scheme, which reached 81%. The probability to wrongly identify a photon in one measurement is 0.029%, which results in a dark rate of $\gamma_{\text{dark}} = 0.116 \cdot 10^{-3} \gamma_a$ assuming a mean rate of $12.5 \cdot 10^{-3} \gamma_a$ incoming photons. Dark counts can be curtailed at the expense of reduced detection efficiency by lowering the threshold value (see also Fig. 8 below). The comparison with the projective measurement toy-model suggest, that improved efficiency at low dark counts may be approached by faster measurements, $\gamma_b/\gamma_a \rightarrow \infty$ and a clearer distinction of measurement outcomes, i.e., a larger displacement β between the respective steady states of cavity b for empty and occupied cavity a . These conditions imply an increase of the Josephson coupling E_J which might lead to the breakdown of the RWA approximation and the validity of the corresponding Hamiltonian Eq. (3). Effects emerging from rotating terms of the Hamiltonian will cause spontaneous excitations in a , drastically increasing the dark rate. Choosing the resonance frequencies of the cavities and other parameters carefully, we can estimate, see Appendix C, that this additional dark rate stays at a similar magnitude as the one found within RWA, so that the general functionality of the device remains at the cost of a reduced operating bandwidth. Furthermore, it is known how far-off resonant non-RWA effects can be curbed by designing the impedance and shape the oscillator resonances [60].

IV. PREAMPLIFICATION FOR IMPROVED DETECTION

Any consideration to further improve the detection efficiency of our measurement scheme has to start by recognizing the hard upper limit of 81% for a resonant Gaussian single-photon pulse achieved by perfect projective measurements stroboscopically repeated at the optimal rate as discussed in Sec. II. One standard approach to improve the efficiency of a nonabsorbing detector is to cascade several measurement units. While the JPD measurement process is indeed nonabsorbing, the strobo-

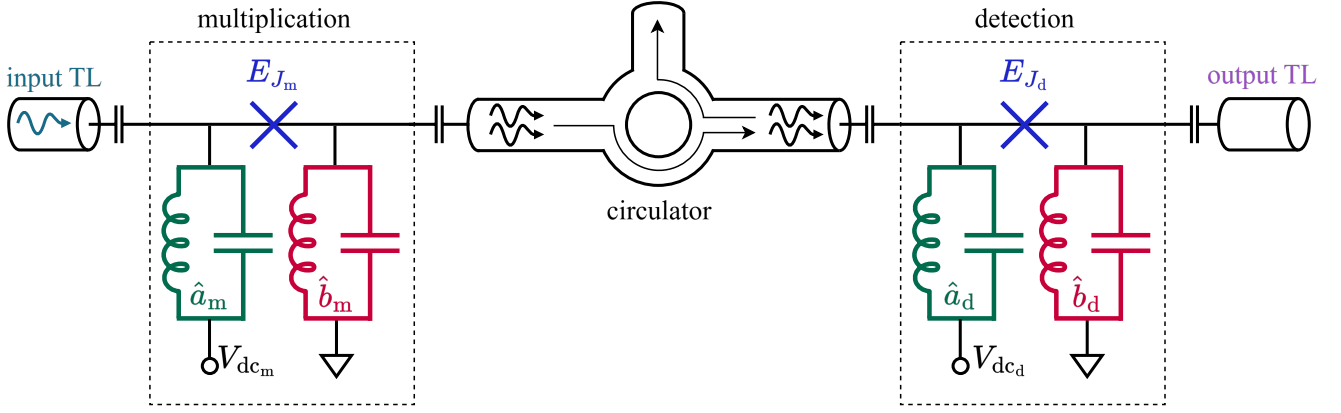


FIG. 7. Schematic detection setup with preamplification by a Josephson-photonics device that works as an inelastic Cooper pair tunneling photon multiplier [48]. One photon impinging from the input transmission line (TL) is absorbed by cavity a_m and multiplied to n photons in cavity b_m by a tunneling Cooper pair when the dc bias fulfills $\omega_{dc_m} + \omega_{a_m} \approx n\omega_{b_m}$ (here $n = 2$). These photons are sent as input into the detection device as described in Sec. III. The circulator ensures that there is no back-scattering from the measurement device on the multiplier.

scopic measurements scatter the photons in a multitude of modes and disturb the shape of the quantum pulse so severely, that any downstream cavity will struggle to absorb the photon and thus cannot accrue further detections.

Instead, we consider a setup, where a single photon pulse is preamplified before being fed into our JPD detector. If two (slightly-delayed) independent photons were produced from a single incoming photon, the detection

limit could go up to $96\% = 1 - (1 - 81\%)^2$. The preamplification scenario is particularly germane, as the very same two-cavity JPD circuit constituting our detector can act as a photon-number amplifier: operated at a biasing condition $2eV_{dc}/\hbar = n\omega_b - \omega_a$ ($n \in \mathbb{N}$) each tunneling Cooper pair creates n excitations into cavity b by annihilating one excitation from cavity a [47, 48, 50]. The Hamiltonian (2) becomes in the appropriate frame and RWA

$$\hat{H}_{J,RWA} \approx \frac{E_J^* \alpha_0 \beta_0^n}{2n!} (\hat{a} \hat{b}^{\dagger n} + \hat{a}^\dagger \hat{b}^n) \quad (11)$$

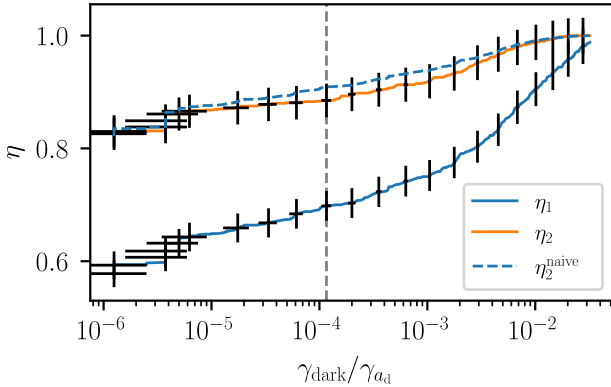


FIG. 8. Detection efficiency η depending on the dark rate γ_{dark} for the simple scheme from Sec. III B (blue) and with the preamplification discussed in Sec. IV (orange). The dashed blue line shows the naive expectation for two independent photons. From left to right, the threshold is increasing, $\sqrt{\gamma_{a_d}} O_{\text{th}} = 2.7 \dots 7$. For parameters see Fig. 6 for the detection JPD and App. D for the preamplifier. The dashed grey line indicates the threshold chosen in Fig. 6(d) to obtain η and γ_{dark} in the main text. The Gaussian input pulse has width $\sigma_\omega/\gamma_{a_d} = 0.1$ (blue); 0.05 (orange). Error bars indicate stochastic uncertainties.

where higher-order corrections similar to the Bessel-functions in (3) and not relevant to our discussion will appear for larger zero-point fluctuations α_0, β_0 . When the Josephson coupling of the multiplier is properly matched to in- and output coupling rates [47], an incoming resonant photon will with near certainty enter the cavity a and be multiplied by a tunneling Cooper pair to n photons in cavity b , which will subsequently leak out of this cavity. The modes of this output and their occupation can be further adjusted by modifying the ratio of input and output coupling, γ_a/γ_b , cf. Ref. [48] and App. D.

As a preliminary to studying the full cascaded set-up shown in Fig. 7 we again turn to our toy-model for the detection process, and consider the preamplifier's output impinging on a cavity, which is stroboscopically subjected to perfect projective measurements. We chose a driving strength E_{J_m} for the multiplier that guarantees near-perfect multiplication [47, 48] and reduce the frequency broadening of the incoming pulse to retain good absorption, as the multiplication device leads to a slight broadening, see App. D.

For a multiplication factor of $n = 2$ a detection probability of $\eta = 95\%$ is reached for the optimal measurement rate (c.f. black dots in Fig. 3), which stays very slightly

below the 96% predicted for two independent photons. Similarly, for $n = 3$ we find 98% (99% respectively).

Results for the full cascaded device shown in Fig. 7 for an $n = 2$ multiplier (orange line) are compared in Fig. 8 to results without preamplification (blue line). Here, for fixed device parameters and weight function the threshold is increased from left to right, yielding increased detection efficiency, but also rising dark rates. The improvement by preamplification is substantial: for instance for a dark rate of $\gamma_{\text{dark}} = 0.116 \cdot 10^{-3} \gamma_{a_d}$ the detection efficiency increases from $\eta_1 = 69.8\%$ without multiplier to $\eta_2 = 88.5\%$ with preamplification.

Note, however, that we show preamplifier results for a photon rate reduced by a factor of two ($6.25 \cdot 10^{-3} \gamma_{a_d}$ necessitated by the reduced frequency broadening of the pulse, see App. D) and that dark counts stemming from spontaneous photon creation in a_d (see Sec. IIIB and App. C) remain a problem.

Due to a large computational effort to simulate the full system, simulations are limited to small multiplication factor $n \lesssim 2$ and an exhaustive investigation of the large parameter space and thorough optimization are beyond the scope of this study. This is particularly regrettable as the naive prediction for two-photon efficiency, $\eta_2^{\text{naive}} = 1 - (1 - \eta_1)^2$ (blue dashed line in Fig. 8) holds surprisingly well. This suggests, that the same argument may be used to calculate n -photon efficiencies for larger multiplication factor n and further improvements towards near-deterministic single-photon detection may be expected.

V. CONCLUSION AND OUTLOOK

We presented a novel scheme to detect a single itinerant microwave photon by stroboscopic projective measurement of a cavity, on which it impinges. We showed that a near-projective measurement can be realized by exploiting the nonlinearity of a Josephson junction, which couples the cavity receiving the photon to a second one within a dc-voltage biased circuit. A driving, which depends on whether the photon has been absorbed by the cavity or not, is induced by the junction on the second cavity, whose output, monitored by homodyne detection, reveals the photon detection.

A toy-model of perfect instantaneous projective measurement was used to find the stroboscopic rate for which repeated measurements maximize the chance of detection, while not curtailing absorption too severely by the quantum Zeno effect.

These results informed the full measurement scheme, where a strong coupling is switched on for short times interrupted by long uncoupled intervals. Choosing a suitable weight function and threshold for the output signal, photon detection efficiencies and dark count rates could be calculated. The detection scheme was amended by using a similar Josephson-circuit as a preamplifier.

Using realistic parameters for the experimental de-

vices, we found, for instance for a dark count rate of $\gamma_{\text{dark}} = 0.116 \cdot 10^{-3} \gamma_{a_d}$, a photon detection efficiency of $\eta_1 = 69.8\%$, rising to $\eta_2 = 88.5\%$ using a preamplifier with a multiplication factor of $n = 2$. In fact, the experimental devices described in this proposal have already been used in the multiplier configuration for the amplification of a (classical) coherent continuous wave input in [49, 50]. Besides the increased complexity of integrating a photon source and extending to the cascaded scenario, the sufficient suppression of unwanted off-resonant processes may be experimentally most challenging. The flexibility of the Josephson-photonics devices will however allow us to easily increase the multiplication factor. In fact, this can in principle be done in-situ by a simple change of the dc voltage of the preamplifier device. In a similar fashion, different resonance conditions can be chosen by the dc voltage of the detector device to activate alternative effective coupling terms between the cavities. Different measurement strategies for these can then be devised and investigated. Progress in the signal analysis can also be made by further optimizing weighting functions and thresholding rules. The versatile platform of Josephson-photonics devices holds high promises and the potential to play a substantial role for the number-resolved detection of itinerant microwave photons.

VI. ACKNOWLEDGEMENTS

MH acknowledges financial support from the Natural Sciences and Engineering Research Council of Canada (NSERC) through grant RGPIN-2025-06130. JA gratefully acknowledges the support of the Deutsche Forschungsgemeinschaft (DFG, German Research Foundation) through AN336/17-1 and AN336/18-1 and the Bundesministerium für Bildung und Forschung BMBF) through QSolid. HZ acknowledges support by the state of Baden-Württemberg through bwHPC and the German Research Foundation (DFG) through grant no INST 40/575-1 FUGG (JUSTUS 2 cluster).

Appendix A: Reverse exponential pulse

For successful photon detection in a projective measurement scheme it is essential, that the interrogated cavity is driven by the impinging pulse to as high a probability of occupation as possible. Indeed, it is well known, that there exists a specific pulse shape, a reverse exponential pulse $u(t) = \sqrt{\gamma_a} \theta(-t) e^{\gamma_a t/2}$, that achieves perfect occupation of the Fock-state $|1\rangle$ at $t = 0$, see Fig. 9 showing pulse shape, perfect reflectionless absorption and the subsequent decay. Intuitively, this observation can be understood as a consequence of time-reversal symmetry: the considered scenario being the time-reverse of the natural decay of cavity with constant loss rate γ_a initialized in $|1\rangle$ to the environment.

Appendix B: Weight function

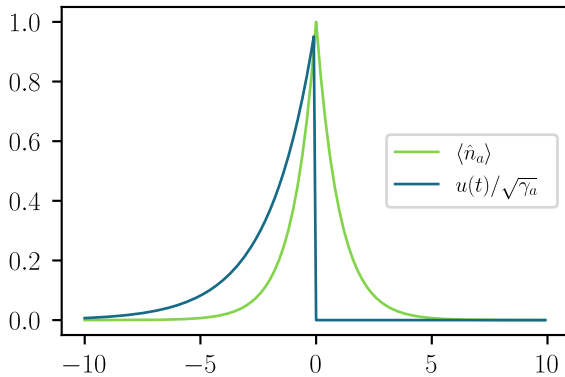


FIG. 9. Occupation of a cavity (green) with loss rate γ_a on which a single photon in a reverse exponential pulse (blue) impinges. Its time constant matches the life time of the cavity. At $t = 0$, the occupation of the cavity reaches unity.

If cavity a is measured projectively once, exactly at $t = t_0$, a photon is detected for sure, $\eta = 100\%$, as indicated by the upper border of the red shaded area in Fig. 3 for $\gamma_m \rightarrow 0$. Increasing the measurement rate and performing several measurements during the pulse disturbs the process of perfect absorption, and the maximal total detection probability decreases. More relevant for a detection scheme is the average over all possible positions of the stroboscopic measurements, for which we found in Fig. 3 (red line) rather low detection efficiencies for the time-reversed exponential, partly explained by its rather wide spectral width which, by construction, cannot be much smaller than the cavity linewidth.

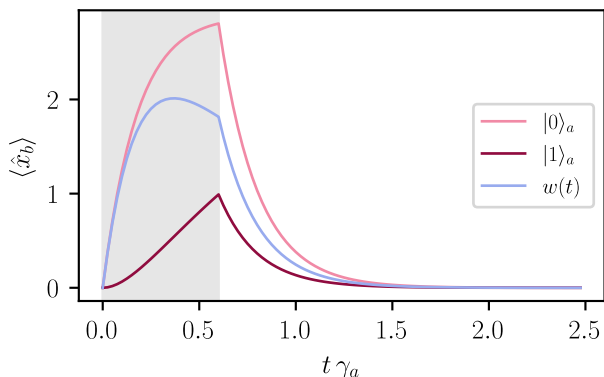


FIG. 10. Expectation values $\langle \hat{x}_b \rangle$ for initial state $|0_a 0_b\rangle$ and $|1_a 0_b\rangle$ according to a Lindblad master equation. The gray area indicates the duration of the measurement ($E_J \neq 0$). The weight function $w(t) = \langle \hat{x}_b \rangle_0 - \langle \hat{x}_b \rangle_1$ is calculated as the difference of the two Lindblad solutions. Parameters as in Fig. 6.

The Measurement outcomes O_j are calculated by a weighted integral over J_{x_b} as shown in Eq. (10). In the following, the origin of the weight function is explained in more detail. Conceptually, it is clear that at the very beginning of the measurement, when E_J is switched on, there is no information in J_{x_b} since in both cases (photon or no photon in a), cavity b starts out in the same state. Therefore, the start of the measurement should be weighted little and the weight should increase while b is approaching its steady state, which is dependent on the state in a .

On the other hand, cavity a is lossy as well. Therefore, the photon in a might get lost while E_J is non-zero which warrants a decrease of the weight towards the end of $E_J \neq 0$. When $E_J = 0$ again, there is still information in the amplitude of b as it needs time to relax back to the vacuum state. During this, the weight function should be non-zero but decay on a scale of γ_b .

To fulfill these specifications, we calculate the weight function as the difference between the expectation values $\langle \hat{x}_b \rangle$ for a Lindblad solution, where the initial state was either $|0_a 0_b\rangle$ or $|1_a 0_b\rangle$, see Fig. 10. Starting from the initial state $|0_a 0_b\rangle$, cavity b approaches its steady state of $|\beta\rangle$ very fast, on a time-scale defined by γ_b , while for $|1_a 0_b\rangle$, this state is reached on the much slower time scale given by the loss of the photon from a with rate γ_a .

Further optimization of the evaluation of the measurement signal, specifically the exact form of the weight function, is left for future work.

Appendix C: Validity of the rotating-wave approximation

As discussed in the main text, the preferred regime for detecting photons with the proposed scheme is a large ratio of γ_b/γ_a , so that the cavity b can quickly adapt to changes of a and therefore approaches an instantaneous measurement. Furthermore, during a measurement the change of amplitudes of \hat{x}_b for $|\psi\rangle_a = |0\rangle$ and $|\psi\rangle_a = |1\rangle$ must be so large that the two states can be distinguished even with the added noise from the homodyne measurement. To fulfill these two conditions simultaneously a large E_J is needed. This, however, puts in doubt the validity of replacing the full (lab-frame) Hamiltonian (2) of the main text, by the RWA-Hamiltonian (3). The validity of the rotating wave approximation is gauged by comparing the scale of E_J with all frequencies, $\omega_a, \omega_b = \omega_{dc}$ and all their sums and differences, such as $|\omega_a - \omega_{dc}|$.

In the rotating frame, the Hamiltonian contains terms of the form $(\hat{a}^\dagger)^k \hat{b}^l$ or $\hat{a}^k \hat{b}^l$ for $l, k \in \mathbb{N}_0$ with prefactor $E_J^*/2\alpha_0^k \beta_0^l$ (and their conjugated complex counterparts). These terms rotate with the frequency $\omega_{rot} = k\omega_{a,rot} - l\omega_{b,rot} \pm \omega_{dc}$ and $\omega_{rot} = -k\omega_{a,rot} - l\omega_{b,rot} \pm \omega_{dc}$, respectively, and are assumed negligible within RWA when $E_J^*/2\alpha_0^k \beta_0^l \ll \omega_{rot}$.

To explain qualitatively which effects the breakdown of the RWA will have on the detection scheme, we exemplarily consider the term proportional to \hat{a} , namely an extra term in the (rotating frame but non-RWA) Hamiltonian,

$$\hat{H}_{\hat{a}} = -i \frac{E_J^* \alpha_0}{2} : \left[\hat{a} e^{-(\omega_{a,\text{rot}} + \omega_{\text{dc}})t} - \hat{a}^\dagger e^{(\omega_{a,\text{rot}} - \omega_{\text{dc}})t} \right] \\ \frac{J_1(2\alpha_0 \sqrt{\hat{n}_a})}{\alpha_0 \hat{n}_a^{1/2}} J_0(2\beta_0 \sqrt{\hat{n}_b}) : . \quad (\text{C1})$$

In case this term is non-negligible, there will be spontaneous excitations in cavity a while performing measurements. These excitations are not distinguishable from itinerant photons getting absorbed by a in our measurement scheme, and therefore these excitations will yield additional incorrect photon counts and increase the dark count rate.

The effects of this specific process along with all other terms and associated processes included in the full time-dependent Hamiltonian (2) are illustrated by Fig. 11, where we compare scenarios with differing γ_a , which effectively sets the bandwidth of detectable photons.

For a fixed central operating frequency ω_a , a higher γ_a implies a larger E_J (as we need to keep $\gamma_a \ll \gamma_b$ and $\beta = E_J^* \beta_0 / (\hbar \gamma_b)$ approximately constant) and, hence, larger non-RWA effects. Indeed, there are significant excitations in cavity a (see the rapidly oscillating dark

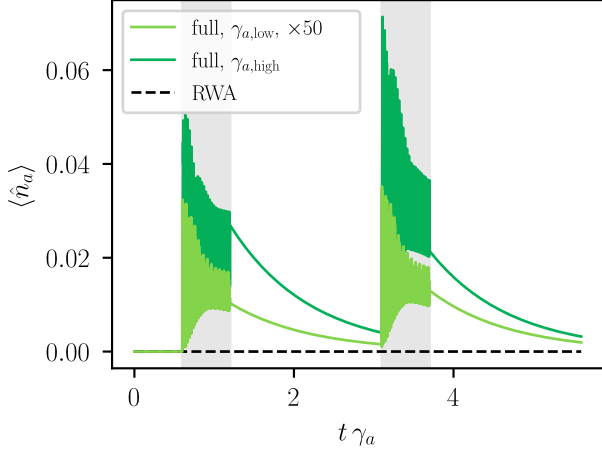


FIG. 11. Occupation $\langle \hat{n}_a \rangle$ according to a Lindblad master equation for two measurements without input pulse. For the RWA Hamiltonian (3), cavity a stays empty since there is no mechanism in the system that could excite the cavity. For low bandwidth (light green), the occupation $\langle \hat{n}_a \rangle$ stemming from the full Hamiltonian (2) closely matches the RWA results with a maximum occupancy of $\langle \hat{n}_a \rangle_{\text{max}} = 7 \cdot 10^{-4}$. For a higher bandwidth (dark green), clear deviations from the RWA are visible with $\langle \hat{n}_a \rangle_{\text{max}} = 0.07$. This would lead to a high dark rate in the investigated measurement scheme.

[Parameters: $\gamma_{a,\text{low}} = 10^{-4} \omega_a$, $\gamma_{a,\text{high}} = 10^{-3} \omega_a$, $\omega_b = 0.76 \omega_a$, other parameters see Fig. 6.]

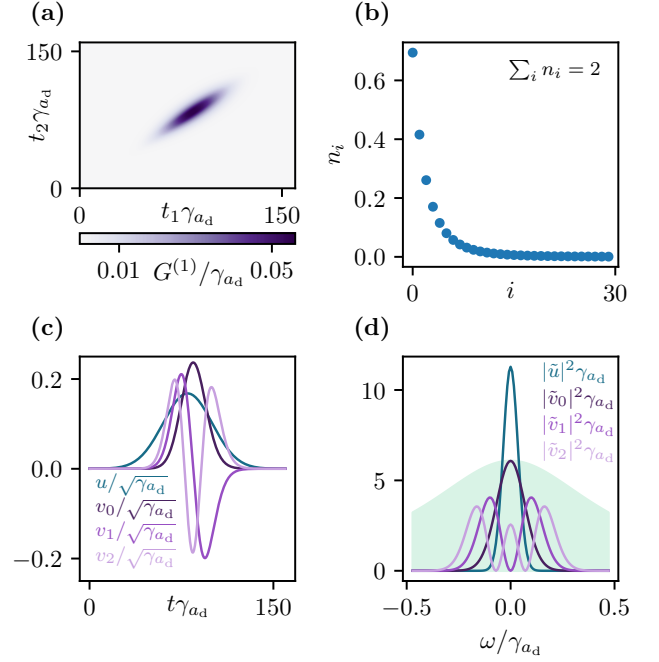


FIG. 12. (a) Autocorrelation function $G^{(1)}(t_1, t_2)$ of the output of the multiplier for multiplication factor $n = 2$. (b) Occupation n_i of the modes found from the diagonalization of $G^{(1)}(t_1, t_2)$. The total occupation across all modes is 2. (c) Temporal mode shapes of input mode $u(t)$ and the three most occupied modes $v_i(t)$, $i = 0, 1, 2$. (d) Frequency spread of input mode $\tilde{u}(\omega)$ and the three most occupied modes $\tilde{v}_i(\omega)$, $i = 0, 1, 2$ in comparison to the resonance curve of cavity \hat{a}_d (turquoise shaded area). [Parameters: $n = 2$, $\gamma_{a_m}/\gamma_{a_d} = 0.5$, $\gamma_{b_m}/\gamma_{a_d} = 0.5$, $\alpha_{0_m} = 0$, $\beta_{0_m} = 0$, $E_{J_m}^* \beta_{0_m}^2 \alpha_{0_m} / (\hbar \gamma_{a_d}) = 1$. For the detection probability in Sec. IV of the main text for $n = 3$: $E_{J_m}^* \beta_{0_m}^3 \alpha_{0_m} / (\hbar \gamma_{a_d}) = \sqrt{9/2}$.]

green line in Fig. 11, and a maximum occupation of $\langle \hat{n}_a \rangle_{\text{max}} = 0.07$ is reached. Moreover, after the first measurement has concluded, the occupation does not fully decay back to zero before the second measurement occurs further increasing the probability of subsequent dark counts. Decreasing γ_a at the cost of lowering the bandwidth strongly suppresses the effects of the rotating terms, and the result follows RWA more closely (light green line). The maximum occupation in this case stays below $\langle \hat{n}_a \rangle_{\text{max}} = 7 \cdot 10^{-4}$. This value can be used as a rough estimate for the probability to detect a photon in a single measurement, without input photon (dark count). In consequence, we expect an additional dark rate, that is not captured by the RWA calculations presented in the main text, of $\gamma_{\text{dark,rot}} = \langle \hat{n}_a \rangle_{\text{max}} \gamma_m = 2.8 \cdot 10^{-4} \gamma_a$, which is of similar order of magnitude as the dark count rate obtained there from the full simulations of the measurement process within RWA.

Appendix D: Multiplier

A preamplification scheme, dubbed as the inelastic Cooper-pair tunneling photon multiplier [47, 50], can be prepended to our detection device. It is a similar Josephson-photonics device with two microwave modes, where the resonance condition is set to $\omega_{d_{c_m}} + \omega_{a_m} \approx n\omega_{b_m}$. Then, an impinging microwave photon is absorbed by cavity a_m and multiplied to n photons in cavity b_m by the energy of one inelastically tunneling Cooper pair. An impedance-matching condition fixes the driving strength $E_{J_m}^* = \hbar\sqrt{\gamma_{a_m}\gamma_{b_m}}\sqrt{n n!}/(\alpha_{0_m}\beta_{0_m}^n)$, where perfect conversion (n photons are emitted from cavity b_m into an output transmission line) can be achieved for a continuous, coherent-state input. For incoming temporal pulses that are sufficiently resonant with cavity a_m (compare Fig. 12), this driving strength still ensures near-perfect conversion. In general, the output of the preamplifier is multimode due to the nonlinear multiplication process. A single incoming photon with frequency $\omega_{in} = \omega_{a_m} \pm \sigma_\omega$ is multiplied to n outgoing photons that are spectrally broadened by the inverse lifetime γ_{b_m} of cavity b_m , because the resonance condition $\omega_{d_{c_m}} + \omega_{a_m} \pm$

$\sigma_\omega \approx n(\omega_{b_m} \pm \gamma_{b_m})$ only fixes the frequency of the sum of the n outgoing photons. By tuning the remaining parameter, $\gamma_{a_m}/\gamma_{b_m}$, the precise output mode structure can be modified. A spectral decomposition of the two-time coherence function $G^{(1)}(t_1, t_2) = \langle \hat{b}_{m,out}^\dagger(t_2)\hat{b}_{m,out}(t_1) \rangle$ of Fig. 12(a) yields the eigenmode occupations and decomposition, c.f. Fig. 12(b, c) of the emitted radiation into the output transmission line [53, 54]. If the photon multiplier itself is used as a photon detector, a regime is favored where a single mode of the output is highly occupied [48]. When used as a preamplifier, we turn to a regime of multiple output modes, c.f. Fig. 12(b). Specifically, these modes are spectrally broader than the original input pulse, Fig. 12(d). If a preamplification step is used, the bandwidth of both devices has to be carefully designed in order to avoid off-resonant reflections of the preamplified signal at the detector. Here, we choose $\gamma_{a_d} = 2\gamma_{a_m}$, such that most of the preamplified signal is still sufficiently resonant with the detector cavity a_d .

REFERENCES

-
- [1] M. Casariego, E. Zambrini Cruzeiro, S. Gherardini, T. Gonzalez-Raya, R. André, G. Frazão, G. Catto, M. Möttönen, D. Datta, K. Viisanen, J. Govenius, M. Prunnila, K. Tuominen, M. Reichert, M. Renger, K. G. Fedorov, F. Deppe, H. van der Vliet, A. J. Matthews, Y. Fernández, R. Assouly, R. Dassonneville, B. Huard, M. Sanz, and Y. Omar, “Propagating quantum microwaves: Towards applications in communication and sensing,” *Quantum Science and Technology*, vol. 8, p. 023001, Mar. 2023.
 - [2] X. Gu, A. F. Kockum, A. Miranowicz, Y.-x. Liu, and F. Nori, “Microwave photonics with superconducting quantum circuits,” *Physics Reports*, vol. 718–719, pp. 1–102, Nov. 2017.
 - [3] Z. Wang, L. Balembois, M. Rančić, E. Billaud, M. Le Dantec, A. Ferrier, P. Goldner, S. Bertaina, T. Chanelière, D. Esteve, D. Vion, P. Bertet, and E. Flurin, “Single-electron spin resonance detection by microwave photon counting,” *Nature*, vol. 619, pp. 276–281, July 2023.
 - [4] J. Travesedo, J. O’Sullivan, L. Pallegoix, Z. W. Huang, P. Hogan, P. Goldner, T. Chaneliere, S. Bertaina, D. Estève, P. Abgrall, D. Vion, E. Flurin, and P. Bertet, “All-microwave spectroscopy and polarization of individual nuclear spins in a solid,” *Science Advances*, vol. 11, p. eadu0581, Mar. 2025.
 - [5] J. O’Sullivan, J. Travesedo, L. Pallegoix, Z. W. Huang, P. Hogan, A. S. May, B. Yavkin, S. Lin, R.-B. Liu, T. Chaneliere, S. Bertaina, P. Goldner, D. Estève, D. Vion, P. Abgrall, P. Bertet, and E. Flurin, “Individual solid-state nuclear spin qubits with coherence exceeding seconds,” *Nature Physics*, vol. 21, pp. 1794–1800, Nov. 2025.
 - [6] E. Albertinale, L. Balembois, E. Billaud, V. Ranjan, D. Flanigan, T. Schenkel, D. Estève, D. Vion, P. Bertet, and E. Flurin, “Detecting spins by their fluorescence with a microwave photon counter,” *Nature*, vol. 600, pp. 434–438, Dec. 2021.
 - [7] E. Billaud, L. Balembois, J. Travesedo, M. Le Dantec, M. Rančić, E. Albertinale, R. Truong, S. Bertaina, T. Chanelière, P. Goldner, D. Estève, D. Vion, E. Flurin, and P. Bertet, “Electron paramagnetic resonance spectroscopy of a scheelite crystal using microwave-photon counting,” *Physical Review Research*, vol. 7, p. 013011, Jan. 2025.
 - [8] A. V. Dixit, S. Chakram, K. He, A. Agrawal, R. K. Naik, D. I. Schuster, and A. Chou, “Searching for Dark Matter with a Superconducting Qubit,” *Physical Review Letters*, vol. 126, p. 141302, Apr. 2021.
 - [9] C. Braggio, L. Balembois, R. Di Vora, Z. Wang, J. Travesedo, L. Pallegoix, G. Carugno, A. Ortolan, G. Ruoso, U. Gambardella, D. D’Agostino, P. Bertet, and E. Flurin, “Quantum-Enhanced Sensing of Axion Dark Matter with a Transmon-Based Single Microwave Photon Counter,” *Physical Review X*, vol. 15, p. 021031, Apr. 2025.
 - [10] A. L. Pankratov, L. S. Revin, A. V. Gordeeva, A. A. Yablokov, L. S. Kuzmin, and E. Il’ichev, “Towards a microwave single-photon counter for searching axions,” *npj Quantum Information*, vol. 8, p. 61, May 2022.
 - [11] S. R. Sathyamoorthy, T. M. Stace, and G. Johansson, “Detecting itinerant single microwave photons,” *Comptes Rendus Physique*, vol. 17, pp. 756–765, Aug. 2016.
 - [12] B. Karimi and J. P. Pekola, “Quantum Trajectory Analysis of Single Microwave Photon Detection by Nanocalorimetry,” *Physical Review Letters*, vol. 124, p. 170601, Apr. 2020.

- [13] B. Karimi, G. O. Steffensen, A. P. Higginbotham, C. M. Marcus, A. Levy Yeyati, and J. P. Pekola, “Bolometric detection of Josephson radiation,” *Nature Nanotechnology*, vol. 19, pp. 1613–1618, Nov. 2024.
- [14] R. Kokkonen, J. Govenius, V. Vesterinen, R. E. Lake, A. M. Gunyhó, K. Y. Tan, S. Simbierowicz, L. Grönberg, J. Lehtinen, M. Prunnila, J. Hassel, A. Lamminen, O.-P. Saira, and M. Möttönen, “Nanobolometer with ultralow noise equivalent power,” *Communications Physics*, vol. 2, p. 124, Oct. 2019.
- [15] R. Kokkonen, J.-P. Girard, D. Hazra, A. Laitinen, J. Govenius, R. E. Lake, I. Sallinen, V. Vesterinen, M. Partanen, J. Y. Tan, K. W. Chan, K. Y. Tan, P. Hakonen, and M. Möttönen, “Bolometer operating at the threshold for circuit quantum electrodynamics,” *Nature*, vol. 586, pp. 47–51, Oct. 2020.
- [16] A. M. Gunyhó, S. Kundu, J. Ma, W. Liu, S. Niemelä, G. Catto, V. Vadimov, V. Vesterinen, P. Singh, Q. Chen, and M. Möttönen, “Single-shot readout of a superconducting qubit using a thermal detector,” *Nature Electronics*, vol. 7, pp. 288–298, Apr. 2024.
- [17] Y.-F. Chen, D. Hover, S. Sendelbach, L. Maurer, S. T. Merkel, E. J. Pritchett, F. K. Wilhelm, and R. McDermott, “Microwave Photon Counter Based on Josephson Junctions,” *Physical Review Letters*, vol. 107, p. 217401, Nov. 2011.
- [18] D. A. Ladeynov, A. L. Pankratov, L. S. Revin, A. V. Gordeeva, A. V. Chiginev, S. A. Razov, and E. V. Il’ichev, “Detection of 5 GHz photons using Al Josephson junctions at 0.7 K,” *Academia Quantum*, vol. 2, June 2025.
- [19] A. Rettaroli, D. Alesini, D. Babusci, C. Barone, B. Buonomo, M. M. Beretta, G. Castellano, F. Chiarello, D. Di Gioacchino, G. Felici, G. Filatella, L. G. Foggetta, A. Gallo, C. Gatti, C. Ligi, G. Maccarrone, F. Mattioli, S. Pagano, S. Tocci, and G. Torrioli, “Josephson Junctions as Single Microwave Photon Counters: Simulation and Characterization,” *Instruments*, vol. 5, p. 25, Sept. 2021.
- [20] G. Oelsner, C. K. Andersen, M. Reháč, M. Schmelz, S. Anders, M. Grajcar, U. Hübner, K. Mølmer, and E. Il’ichev, “Detection of Weak Microwave Fields with an Underdamped Josephson Junction,” *Physical Review Applied*, vol. 7, p. 014012, Jan. 2017.
- [21] J.-X. He, P.-H. Ouyang, Y.-Q. Chai, H. Chang, Q. He, and L.-F. Wei, “Experimental demonstrations of Josephson threshold detectors for broadband microwave photons detection,” *Applied Physics Letters*, vol. 126, p. 202601, May 2025.
- [22] J. Wang, K. Petrovnin, P. J. Hakonen, and G. S. Paraoanu, “Observing the Poisson Distribution of a Coherent Microwave Field With a Parametric Photon Detector,” *IEEE Transactions on Quantum Engineering*, vol. 6, pp. 1–8, 2025.
- [23] B. Fan, G. Johansson, J. Combes, G. J. Milburn, and T. M. Stace, “Nonabsorbing high-efficiency counter for itinerant microwave photons,” *Physical Review B*, vol. 90, p. 035132, July 2014.
- [24] S. R. Sathyamoorthy, L. Tornberg, A. F. Kockum, B. Q. Baragiola, J. Combes, C. M. Wilson, T. M. Stace, and G. Johansson, “Quantum Nondemolition Detection of a Propagating Microwave Photon,” *Physical Review Letters*, vol. 112, p. 093601, Mar. 2014.
- [25] B. Royer, A. L. Grimsmo, A. Choquette-Poitevin, and A. Blais, “Itinerant Microwave Photon Detector,” *Physical Review Letters*, vol. 120, p. 203602, May 2018.
- [26] P. Navez, A. G. Balanov, S. E. Savel’ev, and A. M. Zagoskin, “Quantum electrodynamics of non-demolition detection of single microwave photon by superconducting qubit array,” *Journal of Applied Physics*, vol. 133, p. 104401, Mar. 2023.
- [27] K. Inomata, Z. Lin, K. Koshino, W. D. Oliver, J.-S. Tsai, T. Yamamoto, and Y. Nakamura, “Single microwave-photon detector using an artificial Λ -type three-level system,” *Nature Communications*, vol. 7, p. 12303, July 2016.
- [28] J.-C. Besse, S. Gasparinetti, M. C. Collodo, T. Walter, P. Kurpiers, M. Pechal, C. Eichler, and A. Wallraff, “Single-Shot Quantum Nondemolition Detection of Individual Itinerant Microwave Photons,” *Physical Review X*, vol. 8, p. 021003, Apr. 2018.
- [29] S. Kono, K. Koshino, Y. Tabuchi, A. Noguchi, and Y. Nakamura, “Quantum non-demolition detection of an itinerant microwave photon,” *Nature Physics*, vol. 14, pp. 546–549, June 2018.
- [30] R. Dassonneville, R. Assouly, T. Peronnin, P. Rouchon, and B. Huard, “Number-Resolved Photocounter for Propagating Microwave Mode,” *Physical Review Applied*, vol. 14, p. 044022, Oct. 2020.
- [31] F. Helmer, M. Mariantoni, E. Solano, and F. Marquardt, “Quantum nondemolition photon detection in circuit QED and the quantum Zeno effect,” *Physical Review A*, vol. 79, p. 052115, May 2009.
- [32] V. Gramich, B. Kubala, S. Rohrer, and J. Ankerhold, “From Coulomb-Blockade to Nonlinear Quantum Dynamics in a Superconducting Circuit with a Resonator,” *Physical Review Letters*, vol. 111, p. 247002, Dec. 2013.
- [33] A. D. Armour, M. P. Blencowe, E. Brahim, and A. J. Rimberg, “Universal Quantum Fluctuations of a Cavity Mode Driven by a Josephson Junction,” *Physical Review Letters*, vol. 111, p. 247001, Dec. 2013.
- [34] J. Leppäkangas, G. Johansson, M. Marthaler, and M. Fogelström, “Nonclassical Photon Pair Production in a Voltage-Biased Josephson Junction,” *Physical Review Letters*, vol. 110, p. 267004, June 2013.
- [35] J. Leppäkangas, M. Fogelström, A. Grimm, M. Hofheinz, M. Marthaler, and G. Johansson, “Antibunched Photons from Inelastic Cooper-Pair Tunneling,” *Physical Review Letters*, vol. 115, p. 027004, July 2015.
- [36] A. D. Armour, B. Kubala, and J. Ankerhold, “Josephson photonics with a two-mode superconducting circuit,” *Physical Review B*, vol. 91, p. 184508, May 2015.
- [37] M. Trif and P. Simon, “Photon cross-correlations emitted by a Josephson junction in two microwave cavities,” *Physical Review B*, vol. 92, p. 014503, July 2015.
- [38] T. Aissaoui, A. Murani, R. Lescanne, and A. Sarlette, “A cat qubit stabilization scheme using a voltage biased Josephson junction,” *arXiv:2411.08132*, Dec. 2024.
- [39] M. Hofheinz, F. Portier, Q. Baudouin, P. Joyez, D. Vion, P. Bertet, P. Roche, and D. Esteve, “Bright Side of the Coulomb Blockade,” *Physical Review Letters*, vol. 106, p. 217005, May 2011.
- [40] M. Westig, B. Kubala, O. Parlavecchio, Y. Mukharsky, C. Altimiras, P. Joyez, D. Vion, P. Roche, D. Esteve, M. Hofheinz, M. Trif, P. Simon, J. Ankerhold, and F. Portier, “Emission of Nonclassical Radiation by Inelastic Cooper Pair Tunneling,” *Physical Review Letters*,

- vol. 119, p. 137001, Sept. 2017.
- [41] F. Chen, J. Li, A. D. Armour, E. Brahim, J. Stettenheim, A. J. Sirois, R. W. Simmonds, M. P. Blencowe, and A. J. Rimberg, “Realization of a single-Cooper-pair Josephson laser,” *Physical Review B*, vol. 90, p. 020506, July 2014.
- [42] M. C. Cassidy, A. Bruno, S. Rubbert, M. Irfan, J. Kammhuber, R. N. Schouten, A. R. Akhmerov, and L. P. Kouwenhoven, “Demonstration of an ac Josephson junction laser,” *Science*, vol. 355, pp. 939–942, Mar. 2017.
- [43] C. Rolland, A. Peugeot, S. Dambach, M. Westig, B. Kubala, Y. Mukharsky, C. Altimiras, H. le Sueur, P. Joyez, D. Vion, P. Roche, D. Esteve, J. Ankerhold, and F. Portier, “Antibunched Photons Emitted by a dc-Biased Josephson Junction,” *Physical Review Letters*, vol. 122, p. 186804, May 2019.
- [44] A. Grimm, F. Blanchet, R. Albert, J. Leppäkangas, S. Jebari, D. Hazra, F. Gustavo, J.-L. Thomassin, E. Dupont-Ferrier, F. Portier, and M. Hofheinz, “Bright On-Demand Source of Antibunched Microwave Photons Based on Inelastic Cooper Pair Tunneling,” *Physical Review X*, vol. 9, p. 021016, Apr. 2019.
- [45] A. Peugeot, G. Ménard, S. Dambach, M. Westig, B. Kubala, Y. Mukharsky, C. Altimiras, P. Joyez, D. Vion, P. Roche, D. Esteve, P. Milman, J. Leppäkangas, G. Johansson, M. Hofheinz, J. Ankerhold, and F. Portier, “Generating Two Continuous Entangled Microwave Beams Using a dc-Biased Josephson Junction,” *Physical Review X*, vol. 11, p. 031008, July 2021.
- [46] G. C. Ménard, A. Peugeot, C. Padurariu, C. Rolland, B. Kubala, Y. Mukharsky, Z. Iftikhar, C. Altimiras, P. Roche, H. le Sueur, P. Joyez, D. Vion, D. Esteve, J. Ankerhold, and F. Portier, “Emission of Photon Multiplets by a dc-Biased Superconducting Circuit,” *Physical Review X*, vol. 12, p. 021006, Apr. 2022.
- [47] J. Leppäkangas, M. Marthaler, D. Hazra, S. Jebari, R. Albert, F. Blanchet, G. Johansson, and M. Hofheinz, “Multiplying and detecting propagating microwave photons using inelastic Cooper-pair tunneling,” *Physical Review A*, vol. 97, p. 013855, Jan. 2018.
- [48] L. Danner, M. Hofheinz, N. Bourlet, C. Padurariu, J. Ankerhold, and B. Kubala, “Amplification and Detection of Single Itinerant Microwave Photons,” *arXiv:2510.08030*, Oct. 2025.
- [49] S. Jebari, F. Blanchet, A. Grimm, D. Hazra, R. Albert, P. Joyez, D. Vion, D. Estève, F. Portier, and M. Hofheinz, “Near-quantum-limited amplification from inelastic Cooper-pair tunnelling,” *Nature Electronics*, vol. 1, pp. 223–227, Apr. 2018.
- [50] R. Albert, J. Griesmar, F. Blanchet, U. Martel, N. Bourlet, and M. Hofheinz, “Microwave Photon-Number Amplification,” *Physical Review X*, vol. 14, p. 011011, Feb. 2024.
- [51] U. Martel, R. Albert, F. Blanchet, J. Griesmar, G. Ouellet, H. Therrien, N. Nehra, N. Bourlet, A. Peugeot, and M. Hofheinz, “Influence of bias-voltage noise on the inelastic cooper-pair tunneling amplifier (ICTA),” *Applied Physics Letters*, vol. 126, p. 074001, Feb. 2025.
- [52] Note, however, that the strong scrambling of the photonic mode structure makes a simple cascading impossible, as we will discuss below.
- [53] A. H. Kiilerich and K. Mølmer, “Input-Output Theory with Quantum Pulses,” *Physical Review Letters*, vol. 123, p. 123604, Sept. 2019.
- [54] A. H. Kiilerich and K. Mølmer, “Quantum interactions with pulses of radiation,” *Physical Review A*, vol. 102, p. 023717, Aug. 2020.
- [55] J. Wenner, Y. Yin, Y. Chen, R. Barends, B. Chiaro, E. Jeffrey, J. Kelly, A. Megrant, J. Y. Mutus, C. Neill, P. J. J. O’Malley, P. Roushan, D. Sank, A. Vainsencher, T. C. White, A. N. Korotkov, A. N. Cleland, and J. M. Martinis, “Catching Time-Reversed Microwave Coherent State Photons with 99.4% Absorption Efficiency,” *Physical Review Letters*, vol. 112, p. 210501, May 2014.
- [56] S. Dambach, B. Kubala, and J. Ankerhold, “Generating entangled quantum microwaves in a Josephson-photonics device,” *New Journal of Physics*, vol. 19, p. 023027, Feb. 2017.
- [57] The effective Josephson coupling can be tuned by a magnetic flux, if the junction is realized as a superconducting quantum interference device (SQUID).
- [58] H. M. Wiseman and G. J. Milburn, *Quantum Measurement and Control*. Cambridge: Cambridge University Press, 2009.
- [59] In fact, it is known that voltage fluctuations lead to a slow diffusion of the effective phase of the driving (and the corresponding cavity state in phase space) and how this can be overcome by phase locking [61–63]. For experimental realizations of the detection scheme, we rather envision that we can either monitor a slow phase diffusion and correct the phase of the homodyne quadrature measurement, or straightforwardly adapt our scheme to heterodyne measurement of both quadratures.
- [60] N. Nehra, N. Bourlet, A. H. Esmaili, B. Monge, F. Cyrenne-Bergeron, A. Paquette, M. Arabmohammadi, A. Rogalle, Y. Lapointe, and M. Hofheinz, “DC-powered broadband quantum-limited microwave amplifier,” *arXiv:2512.19902*, Dec. 2025.
- [61] L. Danner, C. Padurariu, J. Ankerhold, and B. Kubala, “Injection locking and synchronization in Josephson photonics devices,” *Physical Review B*, vol. 104, p. 054517, Aug. 2021.
- [62] F. Höhe, L. Danner, C. Padurariu, B. I. C. Donvil, J. Ankerhold, and B. Kubala, “Quantum synchronization in presence of shot noise,” *New Journal of Physics*, vol. 27, p. 023039, Feb. 2025.
- [63] L. Danner, F. Höhe, C. Padurariu, J. Ankerhold, and B. Kubala, “Quantum microwaves: Stabilizing squeezed light by phase locking,” *Physical Review B*, vol. 111, p. 184519, May 2025.